*Journal of The Electrochemical Society*, **147** (3) 803-812 (2000)
S0013-4651(99)05-031-4 CCC: $7.00 © The Electrochemical Society, Inc.


# $^6$Li and $^7$Li Magic-Angle Spinning Nuclear Magnetic Resonance and *In Situ* X-Ray Diffraction Studies of the Charging and Discharging of $Li_xMn_2O_4$ at 4 V

**Young Joo Lee,[a] Francis Wang,[a,b,*] Sanjeev Mukerjee,[c,*] James McBreen,[d,*] and Clare P. Grey[a,*,z]**

[a]*Department of Chemistry, State University of New York at Stony Brook, Stony Brook, New York 11794-3400, USA*
[c]*Department of Chemistry, Northeastern University, Boston, Massachusetts 02115, USA*
[d]*Department of Applied Sciences, Brookhaven National Laboratory, Upton, New York 11793-5000, USA*

$^6$Li and $^7$Li magic-angle spinning (MAS) nuclear magnetic resonance (NMR) and *in situ* X-ray diffraction (XRD) have been used to study lithium manganate cathode materials ($Li_xMn_2O_4$, $0 < x \leq 1$) during and following charging and discharging. Only one major local environment is observed by $^6$Li MAS NMR from 0 to > 50% charging, from lithium in the tetrahedral sites of the spinel structure, the resonance shifting by no more than 8 ppm in this range (from its original position at *ca.* 520 ppm). When the cell is charged above 50%, a new resonance is observed at ≈645 ppm, due to $Li^+$ in a spinel local environment with nearby manganese ions in oxidation states close to +4 (*e.g.,* in a composition such as $Li_{0.1}Mn_2O_4$). The two resonances at ≈520 and 645 ppm are both observed in the range 70 to <80 and 80 to 90% for the samples annealed at 850 and 650°C, respectively. These coexistences occur over the same ranges as the two-phase coexistence, as observed by XRD during the first charging cycle. Resonances were observed at 830 and 930 ppm, for the samples annealed at 650 and 850°C, respectively, at ≥90% charging. These same resonances were seen after multiple charging cycles and are assigned to defect spinels with high manganese oxidation states. Additional resonances are observed for electrodes with high carbon contents at −2 to −13 ppm, from nonspinel phases, which grow in intensity with the number of charging cycles. The presence of the defect spinels and the additional impurity phases contribute to the reduced capacity of these materials. Three-phase behavior is observed by *in situ* XRD during the first discharging cycle. These results are discussed in terms of previous *in situ* XRD charging/discharging results.


Manuscript submitted May 6, 1999; revised manuscript received October 15, 1999.

The lithium manganese oxide spinel, $LiMn_2O_4$, is an inexpensive and environmentally benign intercalation material, which has been widely studied as a promising substitute material for $LiCoO_2$ in the commercial rechargeable battery $Li_xC/LiCoO_2$.[1] The $LiMn_2O_4$ spinel has a three-dimensional structure, consisting of a cubic close packed oxygen array with Mn ions in the 16d octahedral sites and Li ions in the 8a tetrahedral sites.[2,3] This three-dimensional $Mn_2O_4$ lattice provides tunnels that allow lithium-ion diffusion. $Li_xMn_2O_4$ may be deintercalated electrochemically at *ca.* 4 V *vs.* $Li^+/Li$, in the range $0 \leq x \leq 1$, retaining the cubic $Mn_2O_4$ framework throughout. At $x = 0$, the spinel λ-$MnO_2$ is formed; this material has not been synthesized directly by a solid-state reaction.[4,5] Lithium can also be inserted into the interstitial octahedral vacancies (16c) of the spinel structure at *ca.* 3 V *vs.* Li forming $Li_2Mn_2O_4$. This intercalation process induces a Jahn-Teller distortion due to the predominance of $d^4$ $Mn^{3+}$ ions, reducing the $Li_2Mn_2O_4$ crystal symmetry from a cubic to a tetragonal rock salt structure.[4,5] Lithium cations were shown to reside on both 8a and 16c sites in this structure, despite the short Li-Li distance between adjacent 8a and 16c sites.[6,7]

$Li_xMn_2O_4$ suffers from poor cycling behavior after repeated charging and discharging, limiting the life of the cell. Several reasons have been proposed for the capacity fading, including (*i*) a dissolution of the $Li_xMn_2O_4$ electrode in the electrolyte due to a disproportionation reaction that occurs on the surface of the $Li_xMn_2O_4$ particles, $2Mn^{3+} \rightarrow Mn^{4+} + Mn^{2+}_{(solution)}$, (*ii*) the onset of the Jahn-Teller deformation in the deeply discharged state (for $Li_xMn_2O_4$, $x \approx 1$), (*iii*) the presence of an unstable two-phase region at higher potentials (*i.e.,* at $x < 0.45$), and (*iv*) electrolyte decomposition at high potential.[8-14] However, it is still not clear what the most important contributions to the poor cycling behavior are.

Very different cycling behavior has been observed for $Li_xMn_2O_4$, depending on the synthesis conditions and starting materials. For example, lower temperature synthesis introduce higher oxygen content (more cation vacancies) and a higher manganese oxidation state, causing lower capacities but better capacity retention for $Li_xMn_2O_4$ as a ≈4 V electrode ($0 \leq x \leq 1$), in comparison to materials synthesized at higher temperatures. The trends are reversed for the 3 V deintercalation process ($1 < x \leq 2$), and higher capacity is observed for the low temperature syntheses.[15,16]

Lithium manganese oxide spinels show a two-step potential profile in the ≈4 V charge and discharge curves, which may be related to structural changes of the host material. Ohzuku *et al.* proposed, based on early *ex situ* X-ray diffraction (XRD) results, that a two-step topotactic reduction mechanism occurs during the discharging of $Li_{0.27}Mn_2O_4$ to $LiMn_2O_4$: two cubic phases coexist for $0.27 < x < 0.60$ at the 4.10 V plateau in $Li_xMn_2O_4$, and a single cubic phase is observed for $0.60 < x < 1.00$ at the 3.95 V plateau.[4] Xia *et al.* also reported a two-step process at 4 V, but showed that this was suppressed for Li (or oxygen) rich materials.[17] They also linked this two-phase behavior with capacity fading at high potentials.[18] Two-phase behavior has also been observed by Richard *et al.* in their *in situ* XRD studies of lithium-rich spinels.[19] In contrast, Liu *et al.*,[20] based on a combination of neutron diffraction and *in situ* XRD studies, have shown that the discharge of λ-$MnO_2$ (for spinels prepared at 800°C) occurs via a single phase A ($0 < x < 0.2$), then a two-phase coexistence region (A + B: $0.2 < x < 0.4$), a single-phase B ($0.45 < x < 0.55$), and finally a single-phase C ($0.55 < x < 1$). Furthermore, this work suggested that the phase change from B to C is second order, due to the absence of any two-phase coexistence between the two phases. The more recent results of Yang *et al.* obtained at very slow charging rates, confirmed that three-phase behavior occurs for both the stoichiometric and lithium-rich spinels.[21] A two-phase coexistence of phase B and C was observed in the lower-potential plateau in the range $0.6 < x < 0.9$, which suggested that the B and C phase change is first order, and is similar to the phase change observed in the upper potential plateau. The presence of the third phase can be used to explain the two potential plateaus in the electrochemical charge/discharge profiles,[22-24] as well as the two oxidation/reduction peaks observed by cyclic voltammetry. The sharp initial drop in potential on $Li^+$ intercalation in the range $0 < x < 0.1$ is assigned to intercalation into the pure λ-$MnO_2$ spinel phase (phase A), the upper potential plateau arising from the two-phase coexistence of

* Electrochemical Society Active Member.
[b] Present address: Duracell, Needham, MA 02494-2875.
[z] E-mail: clare.grey@sunysb.edu

S0013-4651(99)05-031-4 CCC: $7.00 

phase A and B ($Li_{0.5}Mn_2O_4$). The intercalation of Li ions into a single phase (phase B) results in a rapid lowering of the chemical potential of the Li in the host $Li_{0.5}Mn_2O_4$, resulting in a potential drop of 100 mV, in the range $x \approx 0.5$. Further Li intercalation results in a two-phase coexistence between $LiMn_2O_4$ and $Li_{0.5}Mn_2O_4$ in the lower potential plateau. Again, the chemical potentials of Li in these host cubic spinel phases are similar over a large range, resulting in a flat potential plateau.

A wide variety of other experimental techniques has been used to study these materials, *e.g.*, electrochemistry, transmission electron microscopy (TEM), and X-ray absorption fine structure analysis (XAFS).[4,8,25] Although $^6Li|^7Li$ NMR spectroscopy has been used to study the stoichiometric lithium manganates,[26-31] the method has not been extensively applied to study the materials following charging/discharging. NMR is an ideal method for probing the lithium local structures and electronic states of nearby cations. $^7Li$ NMR spectra of diamagnetic materials are dominated by the quadrupolar interaction and the homonuclear dipolar coupling, and some residual broadening often remains, even under fast MAS conditions.[32] In contrast to $^7Li$, the much smaller quadrupolar moment and weaker homonuclear dipolar coupling of $^6Li$ allows higher resolution spectra with fewer spinning sidebands to be obtained. The paramagnetism of the lithium manganese oxide system, and the consequent interactions between the nuclear and unpaired electron spins complicate the acquisition and interpretation of NMR spectra. However, we and other workers have shown that lithium MAS NMR of these systems can be used to study the local lithium environments in the lithium manganese oxide systems.[26,27,29] A paper showing the $^7Li$ MAS NMR of samples intercalated at 3 V has recently been published.[33] Again, the electron-nuclear dipolar coupling is much smaller for $^6Li$, due to its smaller gyromagnetic ratio, and thus the $^6Li$ spectra of these materials contain many fewer spinning sidebands in the MAS spectra and are easier to interpret. Acquisition of spectra at lower static magnetic fields also results in reduced electron-nuclear dipolar couplings.

We have been exploring the effects of synthesis temperature and defect concentration on the electrochemical behavior of the lithium spinels with NMR and XRD. The goal of this present work is to follow the changes in local structure during and after the charging/discharging and to correlate this with the electrochemical properties, and long-range structure and multiphase behavior, as determined by XRD. $^6Li$ MAS NMR spectra of $Li_xMn_2O_4$ spinels were obtained at several steps of the charging process. *In situ* XRD of lithium manganese spinels synthesized at different temperatures are reported for the same spinel samples, to allow comparison between long-range and local probes of structure under conditions as similar as possible. Preliminary results of our multiple charging studies are presented.

## Experimental

*Sample preparation.*—$LiMn_2O_4$ was prepared in air by the solid-state reaction of $Li_2CO_3$ and $Mn_2O_3$. Stoichiometric amounts of the starting materials were ground together, formed into pellets, and fired at different temperatures. LiMn650 was fired at 650°C for 48 h, and LiMn850 was fired at 650°C for 12 h and then at 850°C for 24 h. [26] $^6Li$ enriched samples were synthesized with $^6Li$ enriched $Li_2CO_3$ (Isotec®; $^6Li > 95\%$). Elemental analyses conducted at Galbraith Laboratories gave Li:Mn molar ratios of 1.00 and 1.02 for the LiMn850 and LiMn650 samples, respectively.

*Electrochemical studies.*—Two sets of compositions for the composite cathodes were used in the experiments. The first set is lower carbon-content electrodes, consisting of spinel powder (LiMn850 or LiMn650) mixed with acetylene black (5 wt %) and poly(vinylidenefluoride) binder (PVDF) (5 wt %). The mixture was then dispersed in 1-methyl-2-pyrrolidinone solvent, coated on aluminum foil and dried under vacuum at 60°C. These electrodes are labeled LiMn850i and LiMn650i. A cathode disk (2.65 $cm^2$) was punched out of the Al foil, weighed, and assembled in the cell. The second method, used in our original preparation of electrodes, involved the spinel phase, acetylene-black, KS2 graphite, and vitreous carbon fiber mixed in a 9:1:5:2 ratio by mass and a poly(tetrafluoroethylene) (PTFE) binder. The components were slurried in ethanol, then rolled into a sheet, dried for approximately 12 h at 70°C, and sintered in an argon atmosphere for 1 h at 300°C. The active material in the final cathode is *ca*. 55 wt %. Two cathode disks (area 2.85 $cm^2$) were punched out per batch. These two types of electrodes are labeled LiMn650ii and 850ii.

The cathode and the lithium foil anode were assembled with a polypropylene separator (Celgard®) into a specially constructed electrochemical cell, designed at Brookhaven National Laboratory, details of which are described elsewhere.[34] Filter paper was used in between the cathode and the Celgard separator to prevent the electrolyte [1.0 M $LiPF_6$ in a 1:1 ethylene carbonate (EC):dimethyl carbonate (DMC) solvent mixture (EM Industries, LP300)] from drying out. The same cell was used for all the experiments.

The charge/discharge experiments were carried out with a battery cycler (Arbin Instruments, College Station, Texas). Charging was typically performed at a current rate of C/8 to C/10. For the NMR experiments on electrodes LiMn650ii and 850ii, the cathode disk was cut into small pieces, which were individually weighed and then placed together again in the same cell. One piece of electrode was extracted after the cell was charged to a certain level. Typically, the cell was left for an hour to reach equilibrium before the cell was disassembled. The cell was then reassembled, and the process was repeated. After each piece of the electrode was extracted, the current was adjusted according to the active mass of cathode remaining in the cell, so that the charging rate of C/8 to C/10 remained constant. (This charging rate corresponds to a current density of 11 to 14 mA/g, depending on the measured capacity of the electrode.) As a control, we also performed experiments where the whole cathode was charged to a specific level, disassembled, and was used in the NMR experiment. This method was used for all low-carbon content electrodes because of the limited cathode material contained in these thinner electrodes.

The extracted cathode was then washed with the solvent mixture to remove the electrolyte residue, prior to the NMR experiments. The amount of deintercalated lithium (the extent of charging) was calculated from the total number of coulombs passed and the weight of the active material present in the electrode by assuming 100% efficiency. Small errors may be introduced into this calculation, however, due to a number of side reactions that can occur, such as electrode surface passivation due to interaction with the electrolyte, and electrolyte decomposition at higher potentials. For the experiments performed on samples after multiple charging/discharging cycles, one cathode was cycled between 3.2 and 4.5 V for 50 times and then cut into pieces for the subsequent charging experiment. Each piece of this cathode was charged to a certain extent, a higher charge cutoff potential of 5 V being used for the fully charged sample.

*Solid-state NMR spectroscopy.*—$^6Li$ MAS NMR experiments were performed at 29.47 MHz on a CMX-200 spectrometer with a double resonance Chemagnetics probe equipped with 3.2 mm rotors for MAS. A $\pi/2$ pulse width of 2.8 μs was used with a 0.24 s delay time, and spectra were recorded with a rotor synchronized echo pulse sequence. $^7Li$ MAS NMR spectra (both one pulse and rotor synchronized echo experiments) were also acquired with the same probe at 77.83 MHz, using a $^7Li$ $\pi/2$ pulse width of 2.4 μs. All spectra were referenced to 1 M LiCl solution, at 0 ppm.

*In situ XRD.*—Studies of the LiMn850ii and LiMn650ii cathodes were performed at the X18A beam line at the National Synchrotron Light Source at Brookhaven National Laboratory. Data were collected with transmission geometry, where the synchrotron X-rays pass through the cell. The diffraction patterns were collected with 10.375 keV ($\lambda = 1.195$ Å) X-rays. The experimental setup is essentially identical to that described in detail elsewhere.[34] The cell was continuously charged or discharged at a C/12 rate, while the XRD powder patterns were acquired. Since the cubic structure of the spinel $Li_xMn_2O_4$ is well known (space group *Fd*3*m*), only a limited $2\theta$ range was recorded (over 32 min), which was chosen so as to

S0013-4651(99)05-031-4 CCC: $7.00 

include the three (511), (440), and (531) Bragg reflections. A full scan between 2θ values of 5 and 53° was taken for every fresh cell before the charge. The sample was allowed to rest for at least 2 h between the charge and discharge. Any zero-point errors in the 2θ values were corrected for by using the reflections due to aluminum in the cell as internal references. The value of $x$ in the formula $Li_xMn_2O_4$ was calculated from the total number of coulombs passed, at each stage of the charging/discharging, and the weight of the active material present in the electrode, by assuming 100% coulombic efficiency, as described above.

## Results and Discussion

*Electrochemistry.*—Figure 1 shows the potential profiles obtained during charging and discharging of the low-carbon cathodes LiMn850i and LiMn650i. The two potential regions are clearly seen. The slightly higher capacity of the material synthesized at a lower temperature (LiMn650i) in the initial charge may be due to the different particle sizes of the cathodes materials; smaller particles are formed at lower temperatures and may allow more efficient lithium ion diffusion and deintercalation.[35] After the first loss in capacity during the first charge/discharge cycle, the capacity of the electrode decreased steadily and was, for example, 97% (≈124 mAh/g) and 70% (≈91 mAh/g) of the initial capacity following discharge, after 4 and 20 cycles, respectively, for LiMn850i. The electrodes prepared with higher carbon contents (LiMn650ii and LiMn850ii) show a much lower capacity during the first charging (90 to 110 mAh/g for LiMn650ii and LiMn850ii, in comparison to 130 to 140 mAh/g for LiMn650i and LiMn850i). There was also a steady decrease in capacity following the first discharge, the LiMn850ii electrode dropping more rapidly. For example, by 50 cycles, the capacity had dropped to 57% of the initial capacity for LiMn850ii (108 mA/g for this particular electrode) and 70% for LiMn650ii. As shown in Fig. 1, the normal two-step potential profile is no longer clearly present after multiple cycles, the potential shifting to higher potential for the charge and to lower potentials for the discharge, at charging rates of C/10 (based on the initial capacity). Thus it is clear that the electrode processing conditions, as well as the intrinsic properties of manganese oxide spinels, play an important role in determining the capacity value and the capacity retention of the electrodes.

*$^6$Li MAS NMR and in situ XRD measurements of $Li_xMn_2O_4$ during the first charge; NMR.*—High resolution $^6$Li MAS NMR spectra were obtained for the LiMn650i cathode charged to different extents (Fig. 2). The spectra of samples following 0 to 75% charging are dominated by a resonance at ≈520 ppm from the lithium cations in the 8a tetrahedral site of the normal spinel phase.[26] At least two less intense resonances are also observed at 0% charging, consistent with our earlier work, where these additional resonances were assigned to lithium ions in normal spinel sites, but near defects in the lattice.[26] No obvious difference in the deintercalation behavior was observed for the three different local environments. These resonances decrease in intensity on charging, as lithium is removed from the structure, but no significant shifts in the resonance frequencies were detected. The spectra shown are of samples following 25 and 75% charging, which represent samples charged to points in the centers of the two potential plateaus in the charging curves (Fig. 1). At 95% charging, which corresponds to a region in the charging curve where the potential has started to rise (the sample was charged to final potential of 4.4 V), the resonance at *ca.* 520 ppm was barely visible, and a new resonance at 648 ppm was clearly visible along with a much less intense resonance at 831 ppm.

Figures 3 and 4 show the $^6$Li MAS NMR spectra of LiMn850ii and LiMn650ii, respectively, at different stages of the electrochemical deintercalation process. Again, the resonance at 520 ppm, due to the 8a tetrahedral site of the normal spinel phase, is observed to shift only very slightly to higher frequency and to decrease in intensity as the cell is charged. For example, the resonance at 518 ppm at 0% charging shifts to 526 ppm by 50% charging for LiMn850ii and from 515 to 520 ppm for LiMn650ii. The resolution of these spectra is much lower than that observed in Fig. 2, and the smaller less intense resonances (at 566 and 605 ppm) are no longer observed. The lower

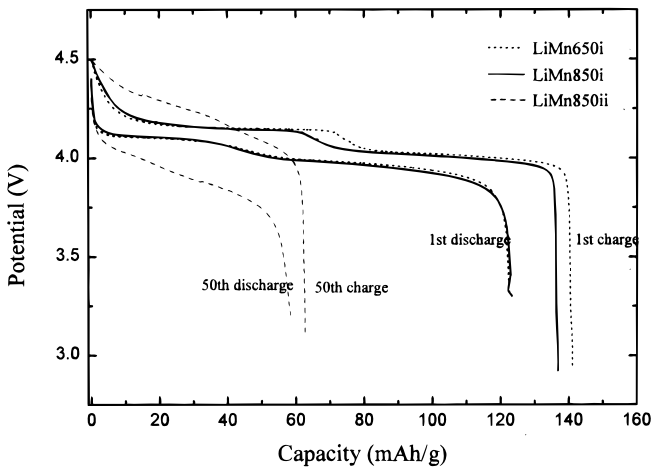


**Figure 1.** Initial charge-discharge profiles (between 4.5 and 3.2 V) for $LiMn_2O_4$ synthesized at different temperatures (LiMn850i and LiMn650i), obtained at a charging/discharging rate of C/10. The 50th charge-discharge curve is also shown for the LiMn850ii electrode.

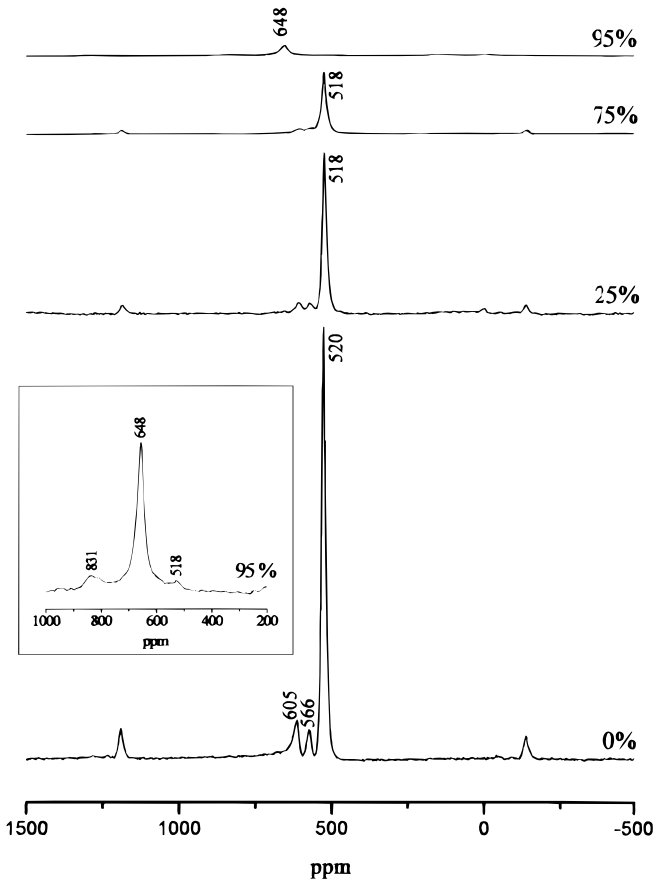


**Figure 2**. *Ex situ* $^6$Li MAS NMR spectra of LiMn650i during the first charging cycle. The spectra were acquired with the rotor-synchronized quadrupolar-echo sequence ($\tau$ = 1 rotor period) with spinning speeds of 20 kHz. The isotropic resonances and the extent of charging are marked on the spectra. All other peaks are spinning sidebands. Spectra are plotted in an absolute intensity scale, taking into account the sample mass and the number of acquisitions; no attempt was made to take into account the changes in relative intensity that may occur due to the different spin-spin ($T_2$) relaxation times.

S0013-4651(99)05-031-4 CCC: $7.00 

resolution is ascribed to the higher carbon contents of these electrodes. A second resonance at 645 ppm was observed for LiMn850ii, along with the resonance at ≈525 ppm at 70% charging. This resonance grows very slightly in intensity from 70 to 80% charging for LiMn850ii. By 80% the resonance at 520 ppm has disappeared, leaving only the resonance at ~640 ppm and a shoulder to lower frequency. A new resonance at 930 ppm is observed at 90% charging. A similar trend was observed for LiMn650ii, where the two resonances at 521 and 642 ppm were observed to coexist from 80 to 90% charging. At 95% charging, the resonance at 637 ppm, along with a higher-frequency resonance, now at 830 ppm, was observed. This is consistent with the $^6$Li NMR of the LiMn650i electrode at the end of the charging curve.

The appearance of resonances at higher frequency, as the charging progresses and the average manganese oxidation state in the spinel phase(s) increases, is consistent with our studies of $Mn^{4+}$ and $Mn^{3.5+}$ model compounds, where $^6$Li (and $^7$Li) NMR resonances were found at higher frequencies for spinels with higher manganese oxidation states;[26] a resonance at 687 ppm was observed for $Li_2Mn_4O_9$ [a vacancy-rich spinel containing Mn(IV)[36-38]] and at 847 ppm for the $Li^+$ ions in the tetrahedral sites in $Li_4Mn_5O_{12}$ [a lithium-rich Mn(IV) spinel[36,37,39]], in contrast to the shift observed for the $Mn^{3.5+}$ spinels at around 520 ppm.[26]

In contrast to the low-carbon-content electrodes, new resonances were observed for LiMn650ii and LiMn800ii at lower frequency (−12 to 91 ppm). The resonance at ~91 ppm is at a shift position typical for a Mn(III) compound.[26] This is consistent with its disappearance after only 5% charging at 4 V. An assignment of the resonances at −2 to −12 ppm is discussed in detail in a later section.

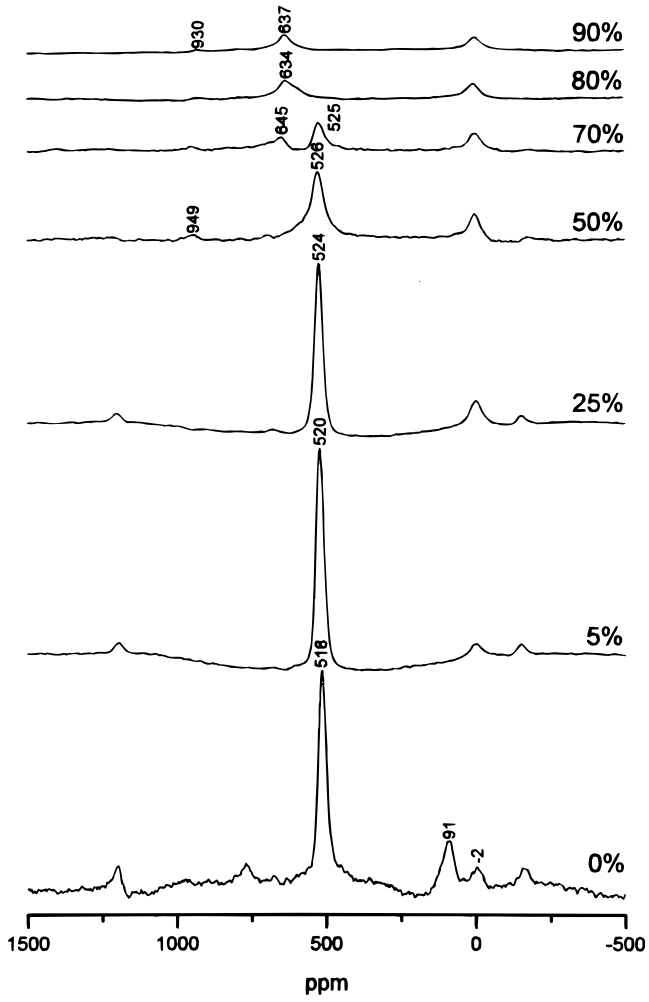


**Figure 3.** $^6$Li MAS NMR spectra of LiMn850ii obtained during the first charging cycle. The spectra were acquired (and are displayed) using the same conditions and methods as those described in Fig. 2.

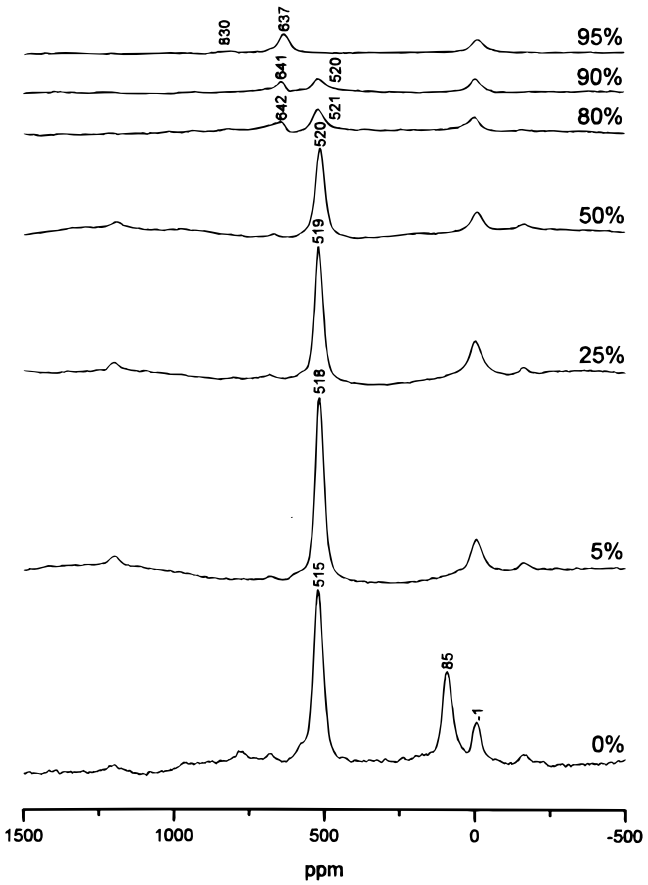


**Figure 4**. $^6$Li MAS NMR spectra of LiMn650ii during the first charging cycle. The spectra were acquired (and are displayed) using the same conditions as those described in Fig. 2.

*XRD.—In situ* XRD patterns obtained during the first charging of LiMn850ii and LiMn650ii are shown in Fig. 5 and 6, respectively (patterns acquired during discharging are shown in Fig. 7 and 8). The changes in the (511), (440), and (531) reflections of the spinel structure were followed to determine the changes in the unit-cell parameters and phases present. As can be seen in Fig. 5, all the reflections gradually shift to larger 2θ values, as the cell is charged. All three Bragg reflections from both samples broaden as charging proceeds in the lower part of the 4 V plateau, but then narrow at around $x \approx 0.5$. The lattice parameter of LiMn650ii drops more slowly, as a function of (average) $x$ than that for LiMn850ii, and there is some evidence for a phase $Li_xMn_2O_4$ with a value for $x$ close to 1 which persists to almost 50% charging. Both samples show clear evidence for two-phase coexistence at high potentials at $0.15 \leq x \leq 0.34$ for LiMn850ii and $0.10 \leq x \leq 0.24$ for LiMn650ii. This behavior is more clearly seen in the plots of lattice parameters (extracted from the 2θ values of the three Bragg reflections) *vs.* charging (Fig. 9). Recent XRD studies involving the LiMn850i cathode are consistent with the behavior of LiMn850ii cathode; a continuous solid solution was observed at low charging potentials, while two-phase coexistence is seen at high potentials.

Both the *in situ* XRD and $^6$Li NMR spectra are consistent with a multiphase deintercalation process during the first charging, involving (at least) two cubic phases with different lithium local structures; the lithium resonance at ≈640 ppm appears at almost identical charging levels ($x \approx 0.3$ for LiMn850 and $x \approx 0.2$ for LiMn650) as the appearance of the low-lithium-content phase by XRD, with a lattice

S0013-4651(99)05-031-4 CCC: $7.00 

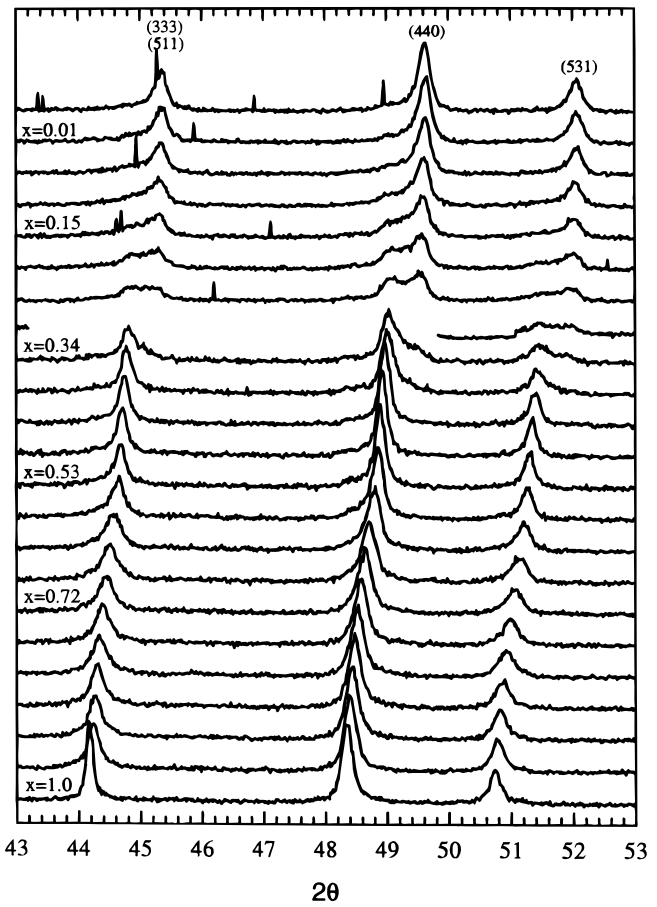


**Figure 5.** *In situ* XRD patterns of the LiMn850ii electrode obtained during charging. The (511), (333), (440), and (531) Bragg reflections of $Li_xMn_2O_4$ were monitored at $x \approx 0.05$ intervals during the first charging of the $Li_xMn_2O_4$ cell. Values for $x$ are indicated on the powder patterns of particular interest. A total capacity for the charge of 108 mAh/g was measured.

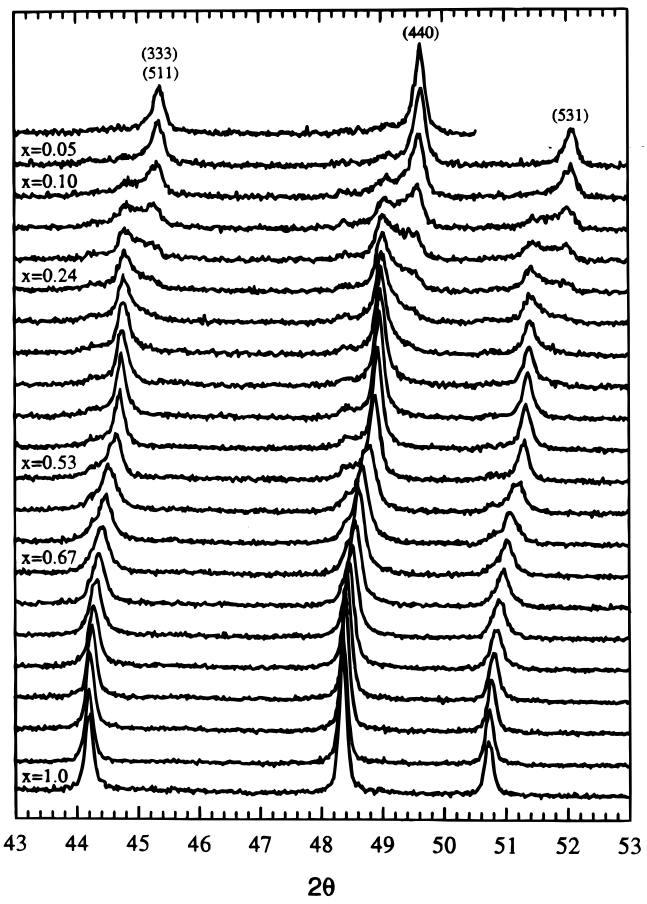


**Figure 6**. *In situ* XRD patterns of the LiMn650ii electrode during charging. Powder patterns are shown at $x \approx 0.05$ charging intervals based on the measured total capacity for the charge of 107 mAh/g.

parameter of ≈8.05 Å (phase A). Thus, this resonance is assigned to lithium ions in phase A. The range of the high-potential two-phase region (as determined by both NMR and diffraction) is different for the materials synthesized at different temperatures; two cubic phases coexist for $0.15 \leq x \leq 0.34$ for the LiMn850 and $0.10 \leq x \leq 0.24$ for the LiMn650 cathodes.

*NMR and XRD measurements obtained during the first discharge.*—The XRD patterns of LiMn650ii and 850ii, during the first discharge, show clear evidence of a two-phase coexistence for both samples in the two intercalation ranges $0.2 < x < 0.5$ and $0.7 < x < 0.9$ (Fig. 7 and 8). The corresponding lattice parameters for these phases, as a function of the extent of intercalation, are plotted in Fig. 9. The cutoff potentials in the discharge were set at 3.3 V in order to avoid the Jahn-Teller active domain and preclude any possibility of tetragonal distortions. The lack of these tetragonal distortions was confirmed by taking a full scan between 2θ limits of 5 to 55° at $\lambda = 1.195$ Å.

The $^6$Li MAS NMR acquired at 80 and 100% discharging of LiMn850i is consistent with the XRD results (Fig. 10); following 100% discharging, a sharp resonance at 518 ppm, due to $LiMn_2O_4$ is clearly visible (along with weaker resonances at ≈830 and 930 ppm). A new resonance at 556 ppm is observed at 80% discharging, which is broader than the resonance of the stoichiometric spinel, suggesting a distribution of local environments.

*Discussion of the multiphase behavior.*—Our XRD results concerning the number of different cubic phases in coexistence with $LiMn_2O_4$ spinels show mixed results for the initial charge. The LiMn850ii sample shows behavior akin to that reported by Liu *et al.*,[18] but does not definitely show the existence of three phases. The broadening of the Bragg reflections on charging, followed by subsequent narrowing at $x \approx 0.5$, does not allow us to rule out completely the presence of an additional phase at $x \approx 0.5$ (phase B). However, our recent results using the LiMn850i electrode showed very little broadening in this range, suggesting that some nonequilibrium effects may contribute to the peak broadening for LiMn850ii. The LiMn650ii sample shows behavior that could be interpreted as evidence of three-phase behavior, with two-phase coexistences in both the upper and lower potential plateaus of the charge curve in the intercalation range $0.10 < x < 0.24$ and $0.53 < x < 1$. However, NMR spectroscopy does not provide any supporting evidence for the three-phase behavior of the stoichiometric spinel; only a small shift of the spinel resonance at ≈520 ppm is observed in the range $x = 1$ to 0.5, and there is no evidence for a new resonance at $x \approx 0.5$. Thus, it appears that no new local lithium environment forms at $x \approx 0.5$, under the charging conditions used in these experiments. Note that this does not totally rule out the presence of more than one phase in this range, only that the NMR is not sensitive to the phase change (*i.e.*, the long range structural change). This appears extremely unlikely, however, given the large shifts observed in these systems. Given the behavior of LiMn850i, it is likely that nonequilibrium effects may also contribute to the behavior of LiMn650ii at low voltages. Thus, we can conclude that we do not see any definitive evidence for two-phase behavior in our systems in the low-potential charging region. This is in contrast to high potentials, where two-phase behavior is clearly seen by both techniques.

Three-phase behavior is seen by XRD during the discharge of both samples. There are also some noticeable differences in the ranges of

S0013-4651(99)05-031-4 CCC: $7.00 

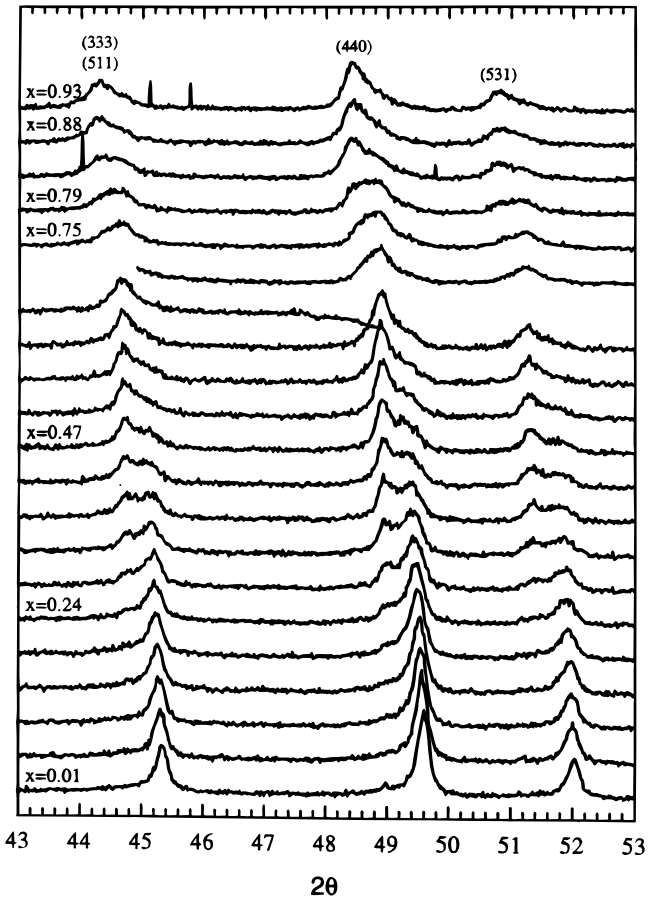


**Figure 7**. *In situ* XRD scans during the first discharging of the LiMn850ii electrode. The powder pattern of $Li_xMn_2O_4$ was collected from $x \approx 0$ to 1. Powder patterns are shown at $x \approx 0.056$ charging intervals.

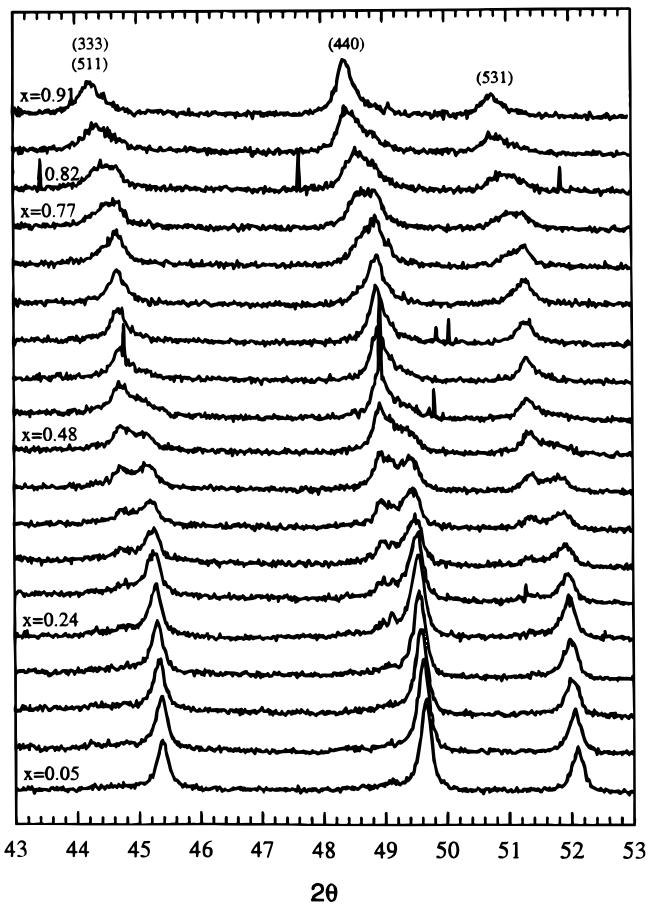


**Figure 8.** *In situ* XRD scans collected during the first discharging of the LiMn650ii electrode. Powder patterns are shown at $x \approx 0.056$ charging intervals.

solid solutions and lattice parameters between charging and discharging, even though identical charge rates were used during charge and discharge. For example, phase A is associated with a much larger change of lattice parameters on discharge (from ≈8.05 to >8.10 Å) for both samples. Phase A is also seen to coexist with the phase with intermediate lithium contents over a larger range than observed during charging. Both samples show a reduced capacity at higher potentials; the sudden drop in potential between the two potential plateaus has shifted and is broader than for charging, occurring from ≈24 to 48% discharging for both samples. This drop is associated with the appearance of the second phase. This phase then persists until more than 80% discharging, where the third phase is observed. Despite the loss in capacity, the third phase is associated with similar lattice parameters as the original stoichiometric spinel, indicating that $Li_{1.0}Mn_2O_4$ is formed at the end of discharge. This is consistent with the $^6$Li MAS NMR, where a sharp resonance at 518 ppm, which is assigned to the stoichiometric spinel, was observed following full discharge.

The material $Li_xMn_2O_4$ ($0.25 < x < 1$) is a phase with a very large solid-solution range. The range of solid solution may be very sensitive to the defect levels. When defects are introduced into $Li_xMn_2O_4$ following charging and discharging, the solid solution ranges of the phases originally close to $x = 0$ and with $0.25 < x < 1$ may no longer remain the same. Furthermore, the kinetics and the thermodynamics of the intercalation process will be altered by the presence of increased defect concentrations, and may also be different for deintercalation and intercalation. In the presence of increased defect concentrations, a slower discharge rate may be required so that equilibrium conditions are achieved during discharge. These nonequilibrium conditions can readily result in apparent two-phase behavior for solid solutions with a large composition range. Our NMR and XRD results suggest that the increased defect concentrations or disorder created by the charge/discharge process may be at least partly responsible for some of the changes in multiphase behavior. More experiments are in progress to try to separate intrinsic multiphase behavior in these systems from nonequilibrium effects more clearly.

*NMR experiments following multiple charging cycles.*—$^7$Li MAS NMR was acquired for the LiMn650ii and LiMn850ii samples following 11 and 50 charge/discharge cycles, in order to explore the causes of the reduced capacity of these electrodes, and to help assign the lower frequency resonances. $^7$Li MAS NMR spectra were acquired for these samples because little of the original $^6$Li enrichment remained following multiple charging cycles. Following 11 cycles, the main resonance at ≈520 ppm has disappeared, and the one-pulse spectrum of the LiMn650ii electrode in the discharged state is dominated by a resonance at 624 ppm (Fig. 11). The resonance at −2 ppm appears to have shifted to −12 ppm. Following 50 charging cycles, the resonance at 624 ppm has disappeared, and two new resonances at 838 and 930 ppm are observed, in the discharged state. The resonance at ≈ −13 ppm has continued to grow in intensity. The one-pulse spectrum of the LiMn850ii electrode following 50 charging/discharging (not shown) is essentially identical, indicating that both samples contain the same defect sites or have the same structure after multiple charging.

In order to determine which lithium resonances observed following 50 cycles correspond to ions that may be deintercalated (at ≈4 V), $^7$Li MAS NMR was performed on sections of the LiMn850ii electrode charged to various levels (Fig. 12). Note that echo experiments were performed to ensure that no broad resonances were lost during data acquisition. This accounts for the differences in appearance of the spectra shown in Fig. 11b and 12 (at 0% charging). A higher capacity of 70 mAh/g was obtained for this electrode during the 51st

S0013-4651(99)05-031-4 CCC: $7.00 

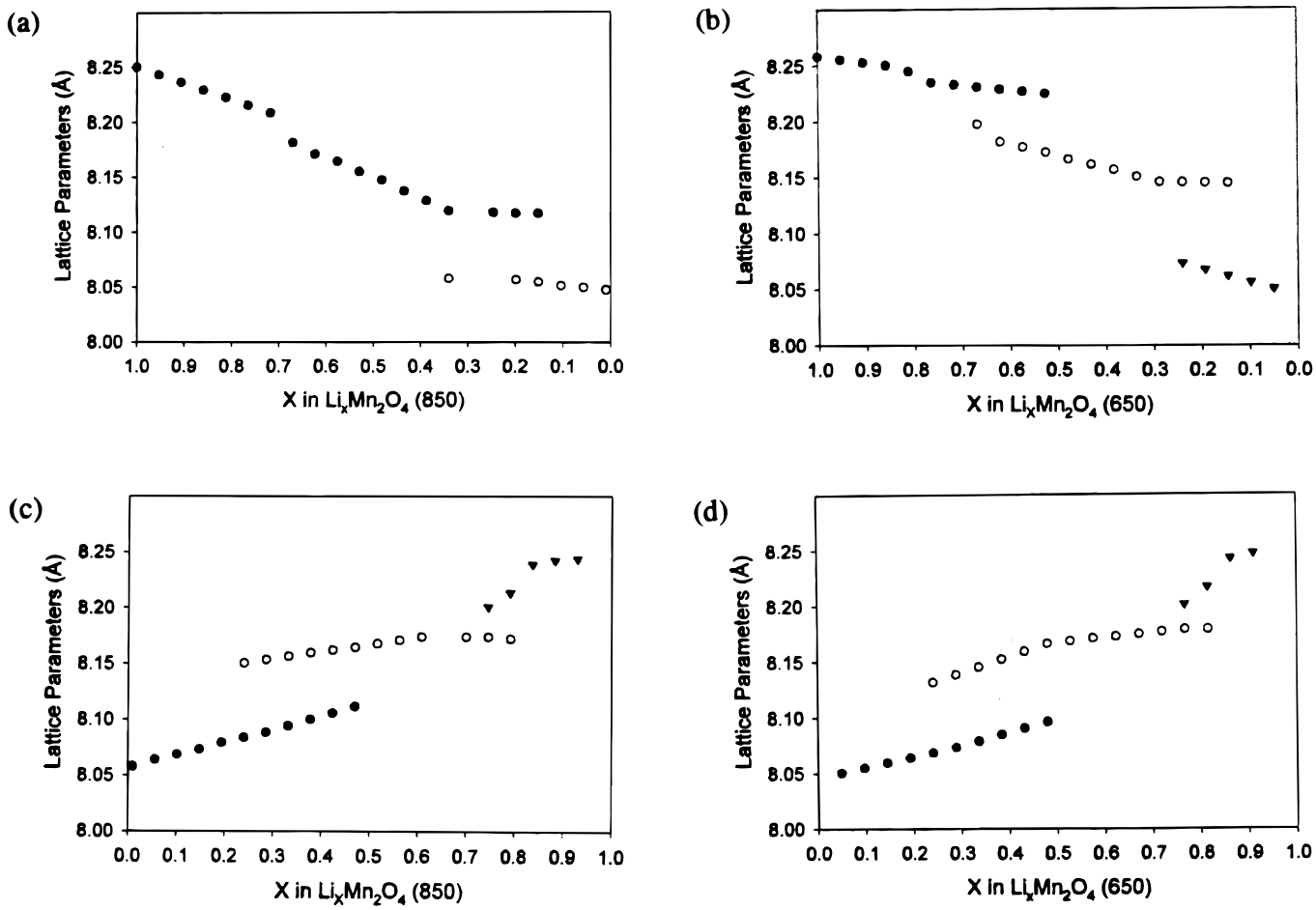


**Figure 9**. Variations in the cubic lattice parameters as a function of the lithium content for (a) LiMn850ii and (b) LiMn650ii during the first charging, and (c) LiMn850ii and (d) LiMn650ii during the subsequent discharging.

charge, in comparison to the capacity results shown in Fig. 1 for the same electrode for the 50th charge. This is due to the higher cutoff potential (5 V) used for this particular experiment. The lithium ions which give rise to a resonance at 930 ppm are deintercalated first. The intensity of the resonance at 838 ppm increases slightly, and a shoulder at *ca.* 765 ppm gradually becomes visible; note that this shoulder may be buried under the broad component in the spectrum of the electrode in the fully discharged state. The lithium species at −13 ppm is not deintercalated following charging. Since it gives rise to approximately 40% of the lithium signal, it is not surprising that these electrodes show a significant reduction in capacity. Thus, one contribution to the loss in capacity comes from the reactions that occur during the processing of the carbon-rich electrode at higher temperatures and during multiple charging cycles, which result in species that resonate between −1 and −12 ppm.

*Assignments of the resonances observed at high frequencies and multiple charging.*—There appear to be (at least) two characteristic resonances (at *ca.* 930 and 830 ppm) that are observed at a higher potential (between 4.3 and 5 V), during the first charging and following multiple charging cycles. These resonances appear to be associated with two defect sites containing $Li^+$, which increase in concentration following multiple charging cycles. One defect is more prevalent, or formed preferentially, in the high-temperature spinel (and results in a resonance at 930 ppm), while the other defect is associated with the lower-temperature material, which is known to contain a higher concentration of defects. These local environments behave very differently during charging of the multicharged electrodes; the environment giving rise to the 930 ppm resonance is deintercalated, while the environment giving rise to the 830 ppm environment increases in intensity, indicating the generation, or population of different cation sites during charging.

One possible compound with the lithium NMR resonances in the same shift range as the two high-frequency resonances is rock-salt-type phase $Li_2MnO_3$, which has three $^6Li$ or $^7Li$ resonances at either 905, 922, and 1817 ppm in one reference[27] or at 850, 875, and 1770 ppm in another.[29] No resonance is observed at ≈1800 ppm in our samples, nor is there any evidence for the formation of this phase by XRD, and thus the two resonances cannot be assigned to $Li_2MnO_3$. Instead, the synchrotron XRD pattern of a sample of LiMn850ii following 50 charging/discharging cycles shows the presence of at least two cubic (spinel) phases and a number of minor, poorly crystalline phases. The two resonances are thus assigned to defect lithium sites in spinel phases.

At least three possible local environments may be envisaged for $Li^+$ in these defects sites: $Li^+$ in 8a, 16d, or 16c sites. If we assume that predominantly Mn(IV) materials are present toward the end of charging, the shifts of both resonances are closest to those for the 8a sites, since much larger hyperfine shifts are predicted for 16c and 16d sites in Mn(IV) spinels.[26,40] For example, our $^6Li$ NMR results of $Li_4Mn_5O_{12}$ and $LiMn_{1.5}M_{0.5}O_4$ (M = Zn or Cu) show resonances at 1800 to 2200 ppm, which are assigned to lithium in the 16d octahedral sites of these predominantly Mn(IV) materials. Thus, the resonance at 830 ppm, whose intensity increases during charging, is assigned to $Li^+$ in a 8a tetrahedral site with one or more nearby manganese or oxygen vacancies, resulting in a defect site. Furthermore, vacancies are highly likely to be present in the original cathode material synthesized at lower temperatures (LiMn650).[26,27] Manganese

S0013-4651(99)05-031-4 CCC: $7.00 

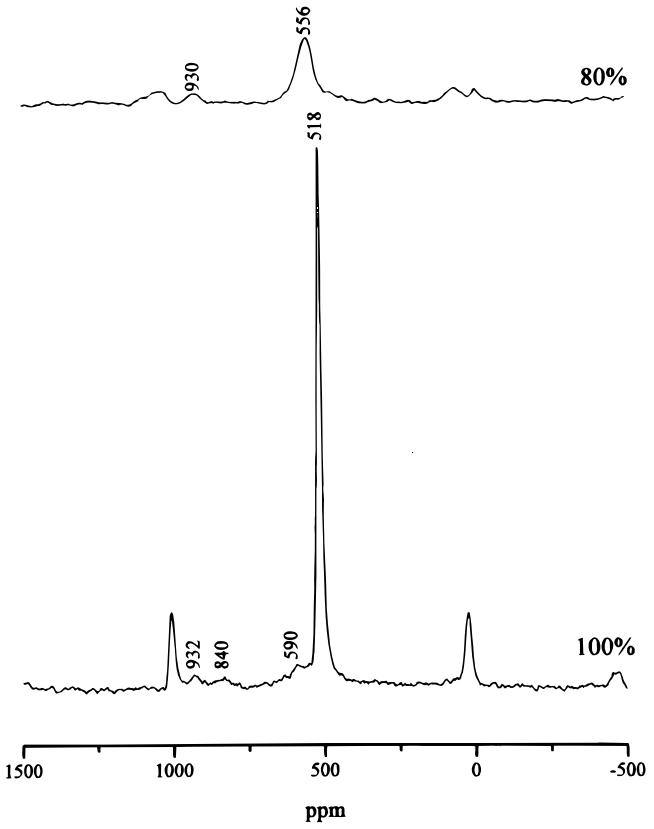


**Figure 10**. $^{6}$Li MAS NMR spectra of LiMn850i during the first discharging cycle. The spectra were acquired with the rotor-synchronized echo sequence ($\tau$ = 1 rotor period) with spinning speeds of 15 kHz. The isotropic resonances and the extent of discharging are marked on the spectra. Spectra are plotted in an absolute intensity scale, taking into account the sample mass and the number of acquisitions; the possible changes in relative intensity that may occur due to the different $T_2$ relaxation times of the resonances were not taken into account.

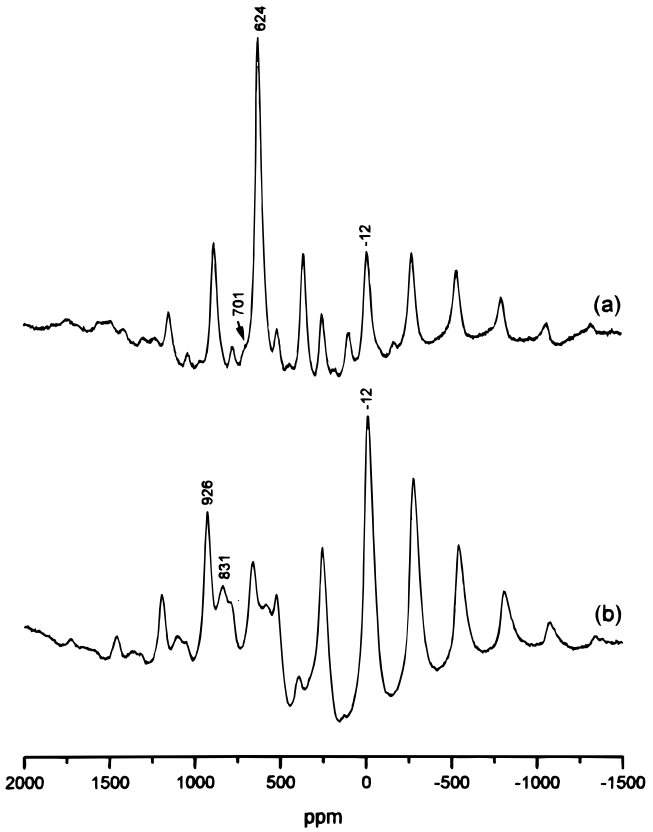


**Figure 11.** $^{7}$Li MAS NMR one-pulse spectra, acquired at the spinning speed of 20 kHz, of the LiMn650ii electrode in the discharged state, after (a) 11 and (b) 50 charge/discharge cycles.

dissolution, which is one proposed mechanism for the capacity fade, results in the formation of manganese deficient phases within the $LiMn_2O_4$-$Li_2Mn_4O_9$-$Li_4Mn_5O_{12}$ phase diagram, suggesting that the cation vacancies are responsible for the defect site.[13] The manganese dissolution mechanism is also consistent with the gradual shift of the spinel resonance from ~520 to 624 to 831 and 930 ppm, following 1, 11, and 50 charging cycles, respectively; this shift is consistent with an increase in the average oxidation state of the spinels. Recently, Shao-Horn *et al.* also suggested the formation of $[Li_zMn_{2-z}]O_4$($0 < z < 0.33$) after cycling the layered $LiMnO_2$ cathode multiple times.[41] Tarascon *et al.* showed two reversible oxidation-reduction peaks at 4.5 and 4.9 V, which are related to local cation defects and are intrinsic to the spinel manganese oxide.[12] They suggested several possible defects; Mn ions in the tetrahedral sites, Li ions in the 16d octahedral sites, or oxidation of octahedral Mn to +5. However, no clear evidence is seen for Li in the octahedral site, surrounded by $Mn^{4+}$, in the charged sample.

It should be noted that not all the manganese ions need necessarily to be in a +4 oxidation state, in all the defect sites, making definite assignments difficult at this point. Indeed, a shift of ≈900 to 1000 ppm is consistent with out predictions for $Li^+$ in the octahedral site of a mixed $Mn^{3+}/Mn^{4+}$ spinel.[26] Furthermore, the fact that the defect associated with the 930 ppm resonance may be deintercalated indicates that there must be a certain concentration of nearby Mn(III) ions associated with this defect. Thus this resonance is assigned to a defect associated with mixed-valent $Mn^{3+}/Mn^{4+}$ ions. Clearly, more work is needed to pin down the exact local structures that give rise to these resonances. Nonetheless, we can conclude that the spinels that remain following multiple charging are no longer stoichiometric defect-free materials, but contain at least two different lithium environments.

*Implications for the electronic structure of $Li_xMn_2O_4$.*—$LiMn_2O_4$ is a small polaron semiconductor, electronic conduction occurring via hopping of electrons between $e_g$ orbitals on adjacent $Mn^{3+}/Mn^{4+}$ cations.[42,43] Thus, the gradual removal of $Li^+$ from the structure during deintercalation should result in a decrease in the number of mobile electrons throughout the whole solid. A gradual shift of the $^{6}$Li/$^{7}$Li resonance to higher frequency during charging might be expected. The NMR spectra are not, however, consistent with this. On the basis of the shifts observed for the Mn(IV) and Mn(+3.5) spinels, significant changes in frequency of more than 80 ppm are predicted to have occurred by 50% charging, which should correspond to an average manganese oxidation state of +3.75. Surprisingly, only a very small shift to higher frequency of approximately 8 ppm is observed as the $Li^+$ is extracted from $Li_xMn_2O_4$ in the range of $x$ = 1 to ≈0.5. This suggests that the local atomic and electronic structure near the lithium ions that remain in the structure does not vary significantly in this range. These results do not appear initially to be consistent with the XRD pattern, where the lattice parameters gradually increase in this charging range, indicating the presence of a continuous solid solution and a smooth change in manganese oxidation state. Our NMR results are, however, consistent with very local structural and electronic perturbations (around the $Li^+$ vacancy) following deintercalation of a lithium ion. The structural perturbations caused by removal of the lithium ion do not appear to affect the Li-O-Mn overlap of the nearby lithium ions (and the lithium ions in the bulk) significantly. The electron associated with $Li^+$ deintercalation cannot be removed from a delocalized band, but must be removed from (or must result in) localized molecular orbitals surrounding the lithium site. The very small change in lithium shift during the first stages of

S0013-4651(99)05-031-4 CCC: $7.00 

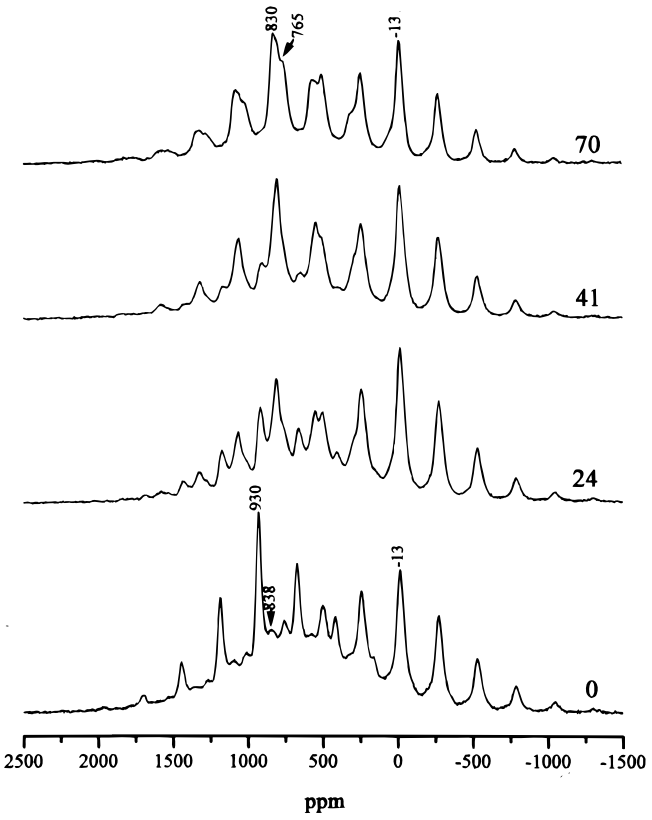


**Figure 12.** $^{7}$Li MAS NMR spectra of LiMn850ii after 50 charge/discharge cycles and following subsequent charging. The spectra were acquired with a rotor synchronized echo-sequence at a spinning speed of 20 kHz. Spectra are plotted in an absolute intensity scale, and the isotropic resonances and the charging extents (in mAh/g units) are marked on the spectra.

charging may also be related to, or consistent with the flat potential profile in this region, since lithium ions are deintercalated from a very similar local environment in this model. These suggestions do not appear to be inconsistent with recent *ab initio* results, which have shown that Li insertion into a λ-$MnO_2$ lattice results in a substantial delocalization of the electron from the Li atom to both adjacent manganese and the oxygen ions.[44,45]

It is difficult to ascribe the NMR results observed during charging to nonequilibrium effects or insufficient relaxation of the electrode prior to acquiring the NMR data; we see no evidence for a second, lithium-depleted phase from 0 to ≈75% charging (containing high-valent manganese ions) by both NMR and diffraction. However, on discharging the electrode, a new resonance is observed at 556 ppm, consistent with a new local environment for $Li^+$, with nearby Mn ions with average oxidation states of greater than 3.5+. Thus it is clear that different local environments for lithium are possible, depending on how the electrode is charged/discharged and the nature of the defects present in the sample. Clearly, further NMR experiments on model compounds, and theoretical calculations, are required to understand this process more fully.

*$Li^+$ in reduced environments in the high-carbon electrodes*.—Two resonances are observed in the low-frequency region, for the spectra of the electrode before charging, at 85 to 91 and −2 ppm for LiMn850ii, and 85 and −1 ppm for LiMn650ii (Fig. 2 and 3). These resonances were not present before processing of the cathode. The resonance at 85 to 91 ppm has disappeared in the electrode following 5% charging, but the resonance at approximately −2 ppm is observed in both samples throughout the charging. The intensity of these resonances varies between sample batches and on the method used to process the electrode. The cathode samples whose spectra contain these resonances have smaller capacities than the cathodes without these resonances. For example, the capacity for LiMn850ii in Fig. 3 and LiMn650ii in Fig. 4 are only 97 and 88 mAh/g, respectively, for the first charge. In contrast, the high-carbon content electrodes whose NMR spectra show much lower intensities of these resonances have capacities of up to ≈100 to 110 mAh/g [*e.g.,* the electrodes LiMn850ii and LiMn650ii used for the *in situ* XRD studies (Fig. 5-9)]. Both resonances were not observed (Fig. 2) in the spectra of the low carbon-content cathode (LiMn650i). Resonances observed at approximately 90 ppm and −1 to −12 ppm cannot be assigned to lithium in $Mn^{3.5+}$ to $Mn^{4+}$ spinels. Resonances at approximately 100 ppm were observed for the Mn(III) compounds $Li_2Mn_2O_4$ and $LiMnO_2$.[26] On this basis, the ≈90 ppm peak may be definitely assigned to a local environment containing Mn(III), of which $Li^+$ in a rock-salt-type ($Li_2Mn_2O_4$) local environment appears the most likely. Mn(III) might be formed during the sintering of the electrode at moderate temperatures under argon gas and in the presence of residual ethanol used in the formation of the slurry. The $Li_xMn_2O_4$ composition range $1.0 \leq x \leq 2$ is not a continuous solid solution, the two phases $LiMn_2O_4$ and $Li_2Mn_2O_4$ coexisting in this range. Thus, even a small level of reduction of the cathode should result in the formation of some $Li_2Mn_2O_4$. Lithium deintercalation of Mn(III) compounds occur between 2.8 and 3.5 V, consistent with the immediate disappearance of this resonance at low charging levels. Evidence was noted by *ex situ* XRD of some of these processed electrodes for shoulders to higher 2θ values of some of the Bragg reflections from the stoichiometric spinel, consistent with the presence of small amounts of additional impurity phases. The intensity of these additional peaks was too small to permit further analysis. We note that additional peaks were not observed for the samples used in the *in situ* XRD experiments, which also showed higher capacities.

The resonance at −1 to −2 ppm, which increases in intensity and shifts to lower frequency (−12 to −13 ppm) as the sample is charged, has not been observed previously for spinel phases. The $Li^+$ that gives rise to this environment is not deintercalated during charging and is responsible for loss in capacity of the electrode. Variable temperature $^{7}$Li MAS NMR experiments of LiMn850ii cycled for 50 cycles were also performed in order to help in the assignments of the resonances. As the temperature is increased, no significant shift in the position of the resonance at −13 ppm is observed, while the resonances in the high-frequency region are very sensitive to temperature, shifting to lower frequency. The Li isotropic chemical shifts for diamagnetic Li compounds range between 3 and −9 ppm,[46] and thus the observed shift is consistent with lithium in a metallic environment or in an environment with only a small hyperfine contribution to the shift. We have observed resonances for lithium in Mn(III) compounds (*e.g.,* orthorhombic $LiMnO_2$) which show only small hyperfine shifts do not have a simple Curie-like dependence on temperature. In this case we have ascribed the behavior to a number of competing shift mechanisms.[40] The $^{7}$Li $T_1$ (3 ms) measurements for the −12 ppm resonance suggests a nondiamagnetic environment. At least two explanations are possible: (*i*) this resonance is due to $Li^+$ ions on the surfaces of the carbon or spinel particles. Results for lithium intercalated into some carbons can lie in this range and are not inconsistent with this suggestion.[47,48] (*ii*) Some nonspinel phases are formed during multiple charging, *e.g.,* a $MnO_2$ phase formed by a disproportionation reaction. The XRD pattern of LiMn850 following multiple charging contains a number of very broad reflections (in addition to the spinel reflections), which may be indexed to the most intense reflections of $MnO_2$ pyrolusite/ramsdellite intergrowth phases, but the data are not good enough to allow more detailed analyses. However, we have observed temperature-independent $^{7}$Li shifts in this range following Li-intercalation into γ-$MnO_2$.[49] γ-$MnO_2$ consists of ramsdellite and pyrolusite intergrowths[50,51] and spinel-ramsdellite and spinel-pyrolusite transformations have been previously reported in the literature.[52-54] A recent transmission electron microscopy (TEM) study of layered $LiMnO_2$, during the initial charge, showed a partial transformation of the layered structure to ramsdellite-$MnO_2$.[41] We are currently synthesizing and acquiring NMR spectra of various $MnO_2$ phases to help test the second suggestion. However,

S0013-4651(99)05-031-4 CCC: $7.00 

the important conclusion that should be made from this section of the work, that is independent of the exact NMR assignments, is that the lithium ions that cannot be deintercalated can be directly seen and quantified by NMR. The change in the concentration and types of lithium ions that are not deintercalated may be readily followed during the charging process.

## Conclusion

NMR may be used to follow the charging and cycling of lithium manganese spinels. In electrodes prepared with high contents of carbon at 300°C, irreversible reactions occur to form nonspinel phases, which are associated with a loss of capacity of the electrode. A Mn(III) compound or local environment is also formed, but lithium ions in this phase are readily deintercalated. No side reactions involving lithium are observed for the electrode processed at lower temperatures with reduced carbon contents. Furthermore, the $^6$Li MAS NMR spectra of these electrodes show much higher resolution (due to the reduced carbon contents), allowing more detailed information concerning the effect of charging on different local environments to be obtained.

The $^6$Li MAS NMR spectra show discrete (hyperfine) shifts as a function of charging level, as opposed to a gradual continuous shift, indicating that there is a distinct number of local environments, with characteristic bonding environments and oxidation states of the nearby manganese ions. This behavior is consistent with the two-plateau regions of the potential *vs.* charging curves, rather than a gradual change in potential. In theory the hyperfine shift of the different resonances should yield further information concerning the electronic structure (as probed by $Li^+$) at each stage of the charging. Two-phase behavior is observed in the high-potential region, by both MAS NMR and XRD diffraction. There is no evidence, however, for two-phase behavior during the low-potential plateau by NMR, at least during charging. The NMR is also extremely sensitive to the presence of $Li^+$ in defect sites; two major resonances associated with $Li^+$ in defect spinels with high manganese oxidation states (approaching +4) are observed at high charging levels. These two resonances increase in intensity following multiple charging, along with the resonances from lithium in nonspinel phases. The conversion of the spinel to the defect and impurity phases is presumably a cause of the loss in capacity in some of our materials. The lithium in the impurity (nonspinel) phase is not deintercalated.

Finally, this paper has demonstrated how sensitive NMR is to the formation of small concentrations of defect phases during and following charging/discharging. Furthermore, NMR can be used to determine the types of defects that are responsible for capacity loss, and are not deintercalated during the charging. Experiments are now in progress to follow the changes in the lithium MAS NMR of electrodes cycled under a wider range of conditions.

## Acknowledgments

Support from the National Science Foundation (to C.P.G.) for the purchase of a solid-state NMR spectrometer (CHE-9405436) and through the National Young Investigator Program (DMR 9458017 and DMR 9901308) is gratefully acknowledged. C.P.G. is an Alfred P. Sloan Research Fellow. An anonymous reviewer is thanked for helpful comments.

*The Alfred P. Sloan Foundation and the NSF assisted in meeting the publication costs of this article.*

## References

1. T. Nagaura and K. Tazawa, *Prog. Batteries Solar Cells*, **9,** 20 (1990).
2. A. F. Wells, *Structural Inorganic Chemistry*, Oxford University Press, Oxford (1993).
3. P. G. Bruce, *Chem. Commun.*, 1817 (1997).
4. T. Ohzuku, M. Kitagawa, and T. Hirai, *J. Electrochem. Soc.*, **137,** 769 (1990).
5. M. M. Thackeray, *J. Electrochem. Soc.*, **142,** 2558 (1995).
6. W. I. F. David, M. M. Thackeray, L. A. de Picciotto, and J. B. Goodenough, *J. Solid State Chem.*, **67,** 316 (1987).
7. M. M. Thackeray, W. I. F. David, P. G. Bruce, and J. B. Goodenough, *Mater. Res. Bull.*, **18,** 461 (1983).
8. R. J. Gummow, A. de Kock, and M. M. Thackeray, *Solid State Ionics*, **69,** 59 (1994).
9. D. H. Jang, Y. J. Shin, and S. M. Oh, *J. Electrochem. Soc.*, **143,** 2204 (1996).
10. G. G. Amatucci, C. N. Schmutz, A. Blyr, C. Sigala, A. S. Gozdz, D. Larcher, and J. M. Tarascon, *J. Power Sources*, **69,** 11 (1997).
11. M. M. Thackeray, Y. Shao-Horn, A. J. Kahaian, K. D. Kepler, E. Skinner, J. T. Vaughey, and S. A. Hackney, *Electrochem. Solid-State Lett.*, **1,** 7 (1998).
12. J. M. Tarascon, W. R. McKinnon, F. Coowar, T. N. Bowmer, G. Amatucci, and D. Guyomard, *J. Electrochem. Soc.*, **141,** 1421 (1994).
13. Y. Xia, Y. Zhou, and M. Yoshio, *J. Electrochem. Soc.*, **144,** 2593 (1997).
14. D. Aurbach, A. Zaban, A. Schechter, Y. Ein-Eli, E. Zinigrad, and B. Markovsky, *J. Electrochem. Soc.*, **142,** 2873 (1995).
15. Y. Xia and M. Yoshio, *J. Electrochem. Soc.*, **144,** 4186 (1997).
16. W. Liu, K. Kowal, and G. C. Farrington, *J. Electrochem. Soc.*, **143,** 3590 (1996).
17. Y. Xia and M. Yoshio, *J. Electrochem. Soc.*, **143,** 825 (1996).
18. Y. Xia, H. Noguchi, and M. Yoshio, *J. Solid State Chem.*, **119,** 216 (1995).
19. M. N. Richard, I. Koetschau, and J. R. Dahn, *J. Electrochem. Soc.*, **144,** 554 (1997).
20. W. Liu, K. Kowal, and G. C. Farrington, *J. Electrochem. Soc.*, **145,** 459 (1998).
21. X. Q. Yang, X. Sun, S. J. Lee, J. McBreen, S. Mukerjee, M. L. Daroux, and X. K. Xing, *Electrochem. Solid-State Lett.*, **2,** 157 (1999).
22. W. Liu, G. C. Farrington, F. Chaput, and B. Dunn, *J. Electrochem. Soc.*, **143,** 879 (1996).
23. R. J. Gummow and M. M. Thackarey, *J. Electrochem. Soc.*, **141,** 1178 (1994).
24. J. B. Goodenough, *Solid State Ionics*, **69,** 184 (1994).
25. Y. Shiraishi, I. Nakai, T. Tsubata, T. Himeda, and F. Nishikawa, *J. Solid State Chem.*, **133,** 587 (1997).
26. Y. J. Lee, F. Wang, and C. P. Grey, *J. Am. Chem. Soc.*, **120,** 12601 (1998).
27. K. R. Morgan, S. Collier, G. Burns, and K. Ooi, *J. Chem. Soc., Chem. Commun.*, 1719 (1994).
28. N. Kumagai, T. Fujiwara, K. Tanno, and T. Horiba, *J. Electrochem. Soc.*, **143,** 1007 (1996).
29. P. Mustarelli, V. Massarotti, M. Bini, and D. Capsoni, *Phys. Rev. B*, **55,** 12018 (1997).
30. B. Gee, C. R. Horne, E. J. Cairns, and J. A. Reimer, *J. Phys. Chem. B*, **102,** 10142 (1998).
31. J. Sugiyama, T. Hioki, S. Noda, and M. Kontani, *J. Phys. Soc. Jpn.*, **66,** 1187 (1997).
32. Z. Xu and J. F. Stebbins, *Solid State Nucl. Magn. Reson.*, **5,** 103 (1995).
33. N. Treuil, C. Labrugere, M. Menetrier, J. Portier, G. Campet, A. Deshayes, J.-C. Frison, S.-J. Hwang, S.-W. Song, and J.-H. Choy, *J. Phys. Chem. B*, **103,** 2100 (1999).
34. S. Mukerjee, J. McBreen, J. J. Reilly, J. R. Johnson, G. Adzic, K. Petrov, M. P. S. Kumar, W. Zhang, and S. Srinivasan, *J. Electrochem. Soc.*, **142,** 2278 (1995).
35. J. M. Tarascon, E. Wang, F. K. Shokoohi, W. R. Mckinnon, and S. Colson, *J. Electrochem. Soc.*, **138,** 2859 (1991).
36. M. M. Thackeray, A. de Kock, M. H. Rossouw, D. Liles, R. Bittihn, and D. Hoge, *J. Electochem. Soc.*, **139,** 363 (1992).
37. C. Masquelier, M. Tabuchi, K. Ado, R. Kanno, Y. Kobayashi, Y. Maki, O. Nakamura, and J. B. Goodenough, *J. Solid State Chem.*, **123,** 255 (1996).
38. A. de Kock, M. H. Rossouw, L. A. de Picciotto, M. M. Thackeray, W. I. F. David, and R. M. Ibberson, *Mater. Res. Bull.*, **25,** 657 (1990).
39. T. Takada, H. Hayakawa, and E. Akiba, *J. Solid State Chem.*, **115,** 420 (1995).
40. Y. J. Lee, C. Eng, and C. P. Grey, In preparation, 1999.
41. Y. Shao-Horn, S. A. Hackney, A. R. Armstrong, P. G. Bruce, R. Gitzendanner, C. S. Johnson, and M. M. Thackeray, *J. Electrochem. Soc.*, **146,** 2404 (1999).
42. H. L. Tuller and A. S. Nowick, *J. Phys. Chem. Solids*, **38,** 859 (1997).
43. J. Sugiyama, T. Atsumi, A. Koiwai, T. Sasaki, T. Hioki, S. Noda, and N. Kamegashira, *J. Phys.: Condens. Matter*, **9,** 1729 (1997).
44. M. K. Aydinol and G. Ceder, *J. Electrochem. Soc.*, **144,** 3832 (1997).
45. M. K. Aydinol, A. F. Kohan, G. Ceder, K. Cho, and J. Joannopoulos, *Phys. Rev. B*, **56,** 1354 (1997).
46. J. W. Akitt, in *The Alkali and Alkaline Earth Metals*, J. Mason, Editor, Chap. 7, Plenum Press, New York (1987).
47. K. Sato, M. Noguchi, A. Demachi, N. Oki, and M. Endo, *Science*, **264,** 556 (1994).
48. Y. Dai, Y. Wang, V. Eshkenazi, E. Peled, and S. G. Greenbaum, *J. Electrochem. Soc.*, **145,** 1179 (1998).
49. Y. Paik, Y. J. Lee, and C. P. Grey, In preparation, 1999.
50. Y. Chabre and J. Pannetier, *Prog. Solid State Chem.*, **23,** 1 (1995).
51. M. M. Thackeray, *Prog. Solid State Chem.*, **25,** 1 (1997).
52. W. I. F. David, M. M. Thackeray, P. G. Bruce, and J. B. Goodenough, *Mater. Res. Bull.*, **19,** 99 (1984).
53. M. M. Thackeray, M. H. Rossouw, R. J. Gummow, D. C. Liles, K. Pearce, A. de Kock, W. I. F. David, and S. Hull, *Electrochim. Acta*, **38,** 1259 (1993).
54. M. M. Thackeray, M. H. Rossouw, A. de Kock, A. P. de la Harpe, R. J. Gummow, K. Pearce, and D. C. Liles, *J. Power Sources*, **43,** 289 (1993).